EMPIRICAL FORMULATION OF BRIDGE INDUCTANCE IN INDUCTIVELY TUNED RF MEMS SHUNT SWITCHES

K. Topalli, M. Unlu, H. I. Atasoy, S. Demir, O. A. Civi and T. Akin

Department of Electrical and Electronics Engineering
Middle East Technical University
Ankara, Turkey

Abstract—This paper presents a substrate independent empirical formulation for the bridge inductance of inductively tuned RF MEMS shunt switches, allowing a systematic design approach to tune their isolation bands. Inductive tuning of RF MEMS switches is achieved by inserting recesses in the ground plane and meanders to the bridges, allowing the tuning of the isolation band of the switch from the X-band to the mm-wave band. The bridge inductance is first extracted from parametric EM simulations of the RF MEMS shunt switches and then fitted to the proposed formulations using empirical coefficients. The accuracy of the formulations is verified with the measurements on the switches that are fabricated using an in-house surface micromachining RF MEMS process on a 500-µm thick glass substrate. Measurement results verify that the bridge inductances can be determined by the provided empirical formulation.

1. INTRODUCTION

RF Microelectromechanical Systems (RF MEMS) have proven their usefulness in microwave applications with their reduced cost, improved performance, and miniaturized dimensions [1]. Among the RF MEMS components, RF MEMS switches [2–6], which show substantially higher performance than semiconductor based counterparts, have an important role for RF MEMS technology, since they are used as a part of many other components, such as phase shifters, impedance tuners, filters, and reconfigurable antennas [7–14]. One of the most important performance criteria of a MEMS switch is the level and bandwidth of

---

Corresponding author: K. Topalli (kagan@metu.edu.tr).

its isolation. The isolation characteristics of conventional MEMS shunt switches show an LC resonant behavior at the mm-wave frequency band. In order to achieve isolation better than 20 dB in X- and Ku-band, the bridge capacitance and/or the bridge inductance should be increased. However, the bridge capacitance is limited due to reasons such as area miniaturization considerations, surface roughness of the used materials, and fabrication difficulties of suspended structures with large areas. The bridge inductance of a conventional MEMS switch is around 5–10 pH, but it can be increased up to 60–70 pH by properly modifying the geometry, which is referred as inductive tuning of a MEMS switch in previous studies [5, 13]. Therefore, these previous studies show that increasing the bridge inductance is an appropriate way of tuning the isolation bandwidth of MEMS shunt switches to X- or Ku-band; however, they do not provide a comprehensive circuit modeling of bridge inductances for designing switches with the required specifications. In this work, a substrate independent formulation for the bridge inductance is derived for the design of inductively tuned RF MEMS switches having recesses in the ground plane and meanders supporting the suspended bridge. The formulation is verified on the manufactured and measured RF MEMS switches. To the authors' knowledge, the empirical formulations relating the MEMS bridge inductance to the physical dimensions are obtained for the first time in the literature. The circuit modeling and empirical formulation of the bridge inductance presented in this work can reduce the design effort by providing a systematic approach in the pre-design phase of RF MEMS switches before proceeding to the EM simulations to complete the design.

2. DESIGN AND MODELING OF INDUCTIVELY TUNED RF MEMS SHUNT SWITCHES

This section presents the design and modeling of inductively tuned RF MEMS shunt switches, by first introducing the various switches designed for modeling the bridge inductance, and then, by showing the circuit model used for modeling the switches. This section also explains how the bandwidth of a shunt switch is specified considering the isolation performance.

2.1. Switch Designs

This work presents three types of switch designs to examine the effect of recesses in the ground plane and meanders supporting the bridge. Fig. 1 shows the top-view of the switches that are designed considering

the in-house surface micromachining RF MEMS process on a 500-µm thick glass substrate; the process details can be found in 14. Fig. 1(a) shows the structure of the switches with standard fixed-fixed beams that are called as Type A switches and are used for comparison purposes with structures with recess. Fig. 1(b) shows the structure of the switches with recessed regions on the ground plane, which is called as Type B switches. The Type B switches have a bridge width of 50 µm or 100 µm, a recess width of 40 or 60 µm with recess depths of 25, 50, 100, or 150 µm. Finally, Fig. 1(c) shows the structure of the switches where the meanders supporting the bridge acts as an additional inductance for the bridge, and this group of switches is called as Type C switches. Here, the primary and secondary meander lengths are defined as w_a (60 µm for both C-1 and C-2) and w_b(100 µm for C-1 and 160 µm for C-2), respectively. The width of the meanders (w_m) is 20 µm. All switches are implemented on coplanar waveguide (CPW) with dimensions of 25/170/25 µm (50 Ω) on the glass substrate ($\varepsilon_r = 4.6$).
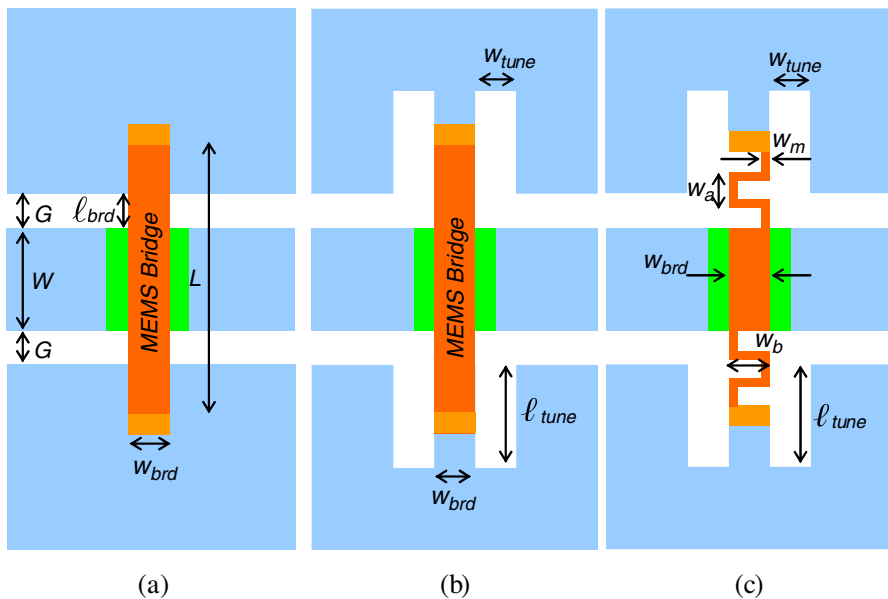
Figure 1. The RF MEMS capacitive shunt switches: (a) Standard (Type A), (b) with the recesses in the ground plane (Type B), and (c) with both recessed ground plane and meanders supporting bridge (Type C).
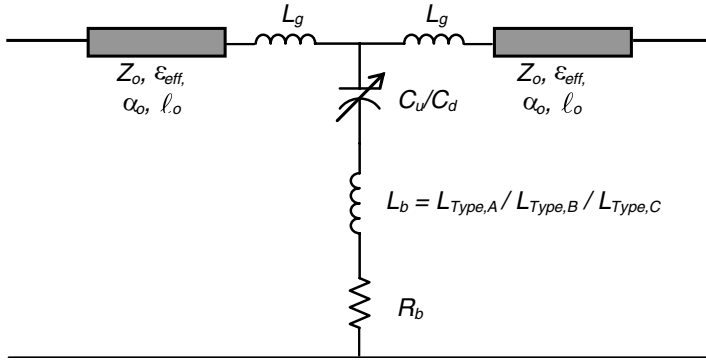
Figure 2. The *CLR* circuit model for the switches presented in this work.

2.2. Circuit Model

Figure 2 shows the circuit model for the RF MEMS switches which is similar to the one in [5]. The model is constructed using two $50\,\Omega$ transmission lines, a shunt *CLR* branch for modeling the bridge, and two series inductances to model the recesses on the ground plane. The bridge inductance in the shunt arm, L_b, is denoted as three different inductances for three types of switches. The series inductor, L_g, models the discontinuity associated with the recesses in the ground plane of the Type B and C switches. This element of the model particularly provides accurate modeling of the upstate characteristics of the Type B and C switches.

2.3. Bandwidth of a Shunt Switch

The bandwidth of a shunt switch is specified considering the isolation performance. The isolation of the switch is limited by the downstate capacitance for the frequencies lower than the LC resonant frequency, f_o, and by the bridge inductance for the frequencies higher than the resonant frequency. Both the bridge inductance, L_b, and the downstate capacitance, C_d, are effective in the vicinity of f_o and specifies two boundary frequencies around the LC resonant frequency. The bridge resistance can be ignored in the bandwidth calculations of each switch. These boundary frequencies are denoted as f_L (or ω_L) and f_H (or ω_H), and they can be solved for $|S_{21}|$ lower than $1/T$ (in decimal), as shown in the following equations:

$$|S_{21}| \leq \frac{1}{T}, \; S_{21}|_{\omega_L} = \frac{1}{T}, \; S_{21}|_{\omega_H} = \frac{1}{T} \tag{1}$$

$$\omega_{L,H} = \frac{1}{2L_b\sqrt{T^2-1}} \left(\sqrt{\frac{1}{C_d}\left(4L_b\left(T^2-1\right)+\frac{Z_o^2 C_d}{4}\right)} \mp \frac{Z_o}{2}\right) \tag{2}$$

$$B = \omega_H - \omega_L = \frac{1}{2L_b\sqrt{T^2-1}}\left(Z_o\right) \tag{3}$$

where Z_o is the characteristic impedance of CPW line ($50\,\Omega$), L_b is the bridge inductance, and T is the specific level of isolation, e.g., $T = 10$ for 20 dB isolation. These equations are used to calculate the boundary frequencies and bandwidth of a shunt switch for a specific isolation level. It is evident from these equations that one can reduce the boundary frequencies and the LC resonant frequency by increasing the bridge inductance, even if the bridge capacitance is kept the same due to the process limitations. However, the increase of bridge inductance reduces the bandwidth of the switch.

3. EXTRACTION OF CIRCUIT MODEL PARAMETERS AND BRIDGE INDUCTANCE FORMULATION

Table 1 presents the dimensions, circuit model parameters, resonant frequency, and boundary frequencies of the switches. The extraction of the circuit model parameters starts with the calculation of the CPW transmission line parameters [15]. The MEMS bridge capacitance in the upstate of the switch, including the fringe fields, is found by [16]:

$$\begin{aligned} C_u \;=\; \varepsilon_0 \Bigg[&1.15\left(\frac{W.w_{brd}}{h_{equ}}\right) + 2.80\left(W + w_{brd}\right)\left(\frac{t}{h_{equ}}\right)^{0.222} \\ &+ 4.12 h_{equ}\left(\frac{t}{h_{equ}}\right)^{0.728} \Bigg] \end{aligned} \tag{4}$$

$$h_{equ} \;=\; g + \frac{t_d}{\varepsilon_r} \tag{5}$$

where, t is the metallization thickness, t_d is the thickness of the isolation dielectric, g is the capacitive gap height, ε_o is the free-space permittivity, and ε_r is the dielectric constant of the isolation dielectric. It is verified with EM simulations that the upstate capacitance of a switch extracted from simulations can be estimated with (4) with an error less than 5%. The downstate capacitance is evaluated using the parallel plate formulation that neglects the fringe field, since the dielectric thickness is very small ($\sim 3000\text{\AA}$).

Table 1. Dimensions, simulated circuit parameters, and frequency bands for isolation better than 20 dB. ($Z_o = 50\,\Omega$, $\varepsilon_{eff} = 2.8$, $\alpha_o = 200\,\text{dB/m}$, height: $2\,\mu\text{m}$).

Type	Dimensions			Circuit model parameters					Frequencies		
	w_{brd} (μm)	ℓ_{tune} (μm)	w_{tune} (μm)	$C_{u,sim}$ (fF)	$C_{d,sim}$ (pF)	L_b (pH)	R (Ω)	L_g (pH)	f_o (GHz)	f_L (GHz)	f_H (GHz)
A-1	50	-	-	47	1.75	5.7	0.1	0	50.1	26.1	96.7
A-2	80	-	-	73	2.8	3.6	0.1	0	49.9	19.3	131
B-1	50	100	40	47	1.75	18.8	0.1	15	27.6	18.7	40.3
B-2	50	50	40	47	1.75	11.4	0.1	12	35.6	21.6	57.3
B-3	50	25	40	47	1.75	8.3	0.1	6	42	24.1	73.1
B-4	100	150	40	90	3.5	17.2	0.08	25	20.4	11.7	35.9
B-5	100	150	60	90	3.5	20	0.06	35	19.1	11.3	32.6
C-1	100	150	60	90	3.5	49.8	0.2	35	12	8.6	16.7
C-2	160	150	60	142	5.6	61.7	0.2	55	8.4	5.8	12.4

The series inductance, L_g, and bridge resistance, R_b, are evaluated using the curve fitting techniques on the EM simulated (Ansoft HFSS) or measured characteristics. The series inductance, L_g, can be extracted using the return loss characteristic of the switch in the upstate. The series resistance of the bridge can be best extracted from $|S_{21}|$ at the LC resonant frequency, since the shunt branch reduces to a simple resistance at resonance in the downstate. The series resistance of the switches is usually lower than $0.3\,\Omega$, which is very low compared to semiconductor switches.

The bridge inductance, L_b, models the voltage induced on the bridge due to the current flowing to the ground planes. The inductance is determined by the portion over the gaps of the CPW since the fields are concentrated at the gaps, and there is a canceling effect for the portions of the bridge over the CPW center conductor and ground planes [5].

The empirical formulation for the bridge inductance presented in this study is based on the extracted inductance values of the switches from curve fitting between the circuit model and EM simulations. The results show that the bridge inductances extracted from the presented switches vary from $3.6\,\text{pH}$ to $61.7\,\text{pH}$. Even this large variation should be modeled with an accurate empirical formulation to have a systematic approach in the design of inductively tuned RF MEMS switches, which is the case for this work, as presented in detail below.

The inductance of the bridge can be enhanced by decreasing the width (w_{brd}) and increasing the length of the bridge (ℓ_{brd}) over the CPW gaps [5]. The bridge inductance for the Type A switches for the given dimensions, L_A, can be related to the physical dimensions as:

$$L_A = L_1 = c_1 \frac{\ell_{brd}}{w_{brd}} \tag{6}$$

where c_1 is an empirical coefficient and determined to be 11.4 by curve fitting to the values in Table 1. The length of the bridge (ℓ_{brd}) over the CPW gaps is directly equal to the gap (G) of the CPW for the Type A switches.

The recessed section in the Type B switches constitutes a short circuited CPW transmission line with a length equal to the recess depth, ℓ_{tune} [5]. The characteristic impedance of the short circuited line, $Z_{recess,}$ depends on both the width of the bridge (w_{brd}) and the width of the recess (w_{tune}). Using the short-length approximation, the CPW line between the anchor of the bridge and the ground planes can be modeled as an inductance series to the bridge, which is directly proportional to Z_{recess} and ℓ_{tune}:

$$L_2 \propto Z_{recess}\left(w_{tune}, w_{brd}\right) \times \ell_{tune} \tag{7}$$

By curve fitting to the values in Table 1 to define the proper equation in the form of (7), the inductance due to the recesses in the ground plane can be expressed as:

$$L_2 = c_2\left(\ell_{tune} - c_3\right) \sqrt{\frac{w_{tune}}{w_{brd}}} \tag{8}$$

where c_2 and c_3 are empirical coefficients with values of 0.16 and 7.2, respectively. The calculated characteristic impedance of the recessed section, $Z_{recess,}$ shows a similar dependency with the width of the bridge (w_{brd}) and the width of the recess (w_{tune}). The bridge inductance for Type B switches, L_B, is the sum of L_1 and L_2:

$$L_B = c_1 \frac{\ell_{brd}}{w_{brd}} + c_2\left(\ell_{tune} - c_3\right) \sqrt{\frac{w_{tune}}{w_{brd}}} \tag{9}$$

If the width of the bridge over the CPW gap is reduced and the length of the bridge is increased by employing meanders, the inductance can significantly be enhanced. In order to express the contribution of the meander to the bridge inductance, (6) is modified as:

$$L_3 = c_4 \frac{w_A + 2w_B}{w_m} \tag{10}$$

where c_4 is an empirical coefficient, which is determined to be 2.5. The numerator of the expression is nearly equal to the total length of the

meander by neglecting the connection sections at the anchor and the bridge, which are only 20 μm each. The bridge inductance for Type C switch, L_C, is the sum of L_2 and L_3:

$$L_C = c_2 \left(\ell_{tune} - c_3\right) \sqrt{\frac{w_{tune}}{w_{brd}}} + c_4 \frac{w_A + 2w_B}{w_m} \qquad (11)$$

Equations $(6), (9), (11)$ relate the physical dimensions of the switches to the bridge inductances including 61.7 pH. Higher inductance values might be targeted by using longer meanders than the ones used in the Type C-2 switch; however, this will increase buckling associated problems in the meanders and the bridge. Therefore, in this study, the inductance values larger than 60–70 pH are not considered in the empirical formulation of the inductances.

In order to evaluate the validity of the empirical formulation of bridge inductances for different substrate permittivities, simulations are repeated on a 500-μm thick high-resistivity silicon substrate ($\varepsilon_r = 11.9$). The CPW dimensions are modified as 60/100/60 in order to obtain a 50 Ω transmission line on the high-resistivity silicon substrate. The extracted inductances from the simulations show that the inductances due to the recesses and meanders are nearly independent of the substrate permittivity, which allow us to keep the same coefficients and expressions for L_2 and L_3. Although the basic bridge inductance, L_1, shows a slight dependency on the substrate permittivity, this dependency can simply be included in the corresponding equation by modifying c_1 as 8.1. These analyses on the glass and high-resistivity silicon substrates indicate that the empirical formulations for the bridge inductance given in this study are valid for a wide range of substrate permittivity, for the major contributors to the bridge inductance in particular, i.e., recesses and meanders.

4. MEASUREMENT RESULTS

The proposed circuit model is verified on the switches that are fabricated using the in-house surface micromachining RF MEMS process on a 500-μm thick glass substrate [14]. Fig. 3 shows the photograph of the fabricated switches and Fig. 4 the SEM photographs of a Type C-2 switch along with a close up view of its meander section. The RF measurements of the switches are performed using the HP 8720 D vector network analyzer for 1–20 GHz band with the SOLT calibration. A Picosecond 5542-230 bias-tee is used to apply the actuation voltage. A number of measurements are conducted to evaluate the accuracy of the circuit model and the performance of the fabricated switches.
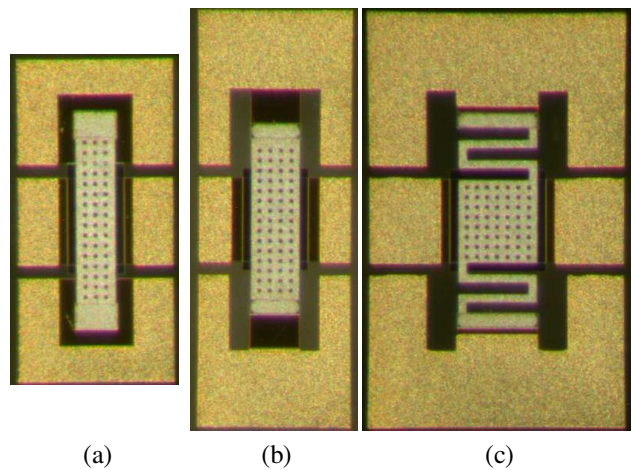
Figure 3. The photographs of the fabricated switches: (a) Type A-2, (b) Type B-5, (c) Type C-2.
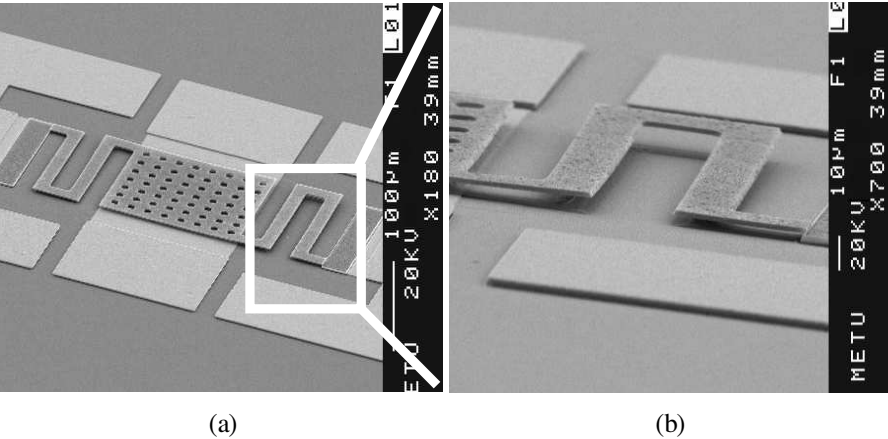
Figure 4. The SEM photographs of the fabricated structures: (a) The overall view of the Type C-2 switch and (b) close up view of its meandered section.

4.1. Evaluation of the Circuit Model

Table 2 gives the bridge height measured by the surface profiler and the upstate-downstate capacitance values of the switches extracted from the RF measurements by curve-fitting the circuit model to the measurement results. Fig. 5 shows the measured and modeled S-
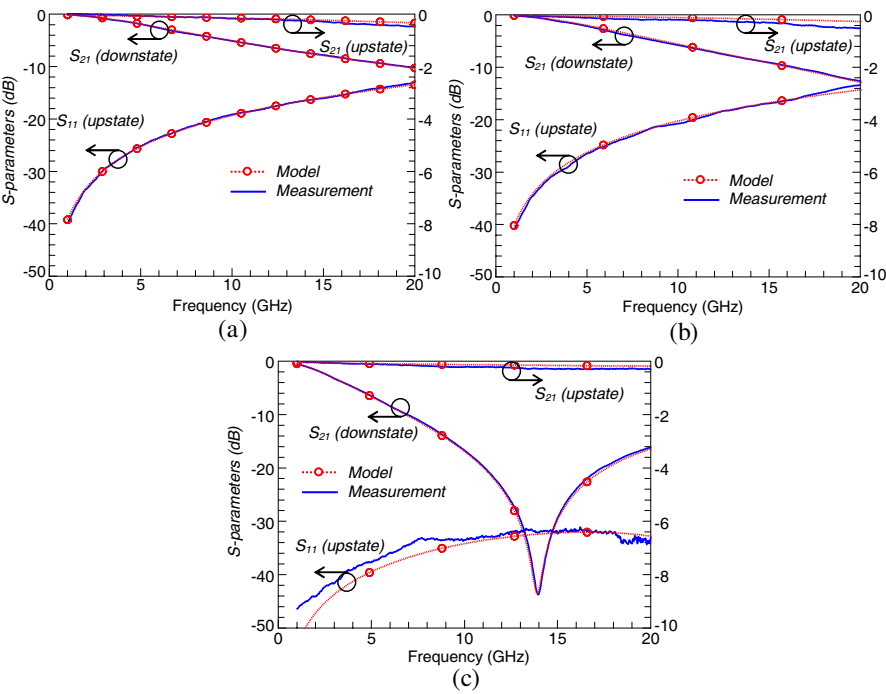
Figure 5. The measurement results for the switches: (a) Type A-2, (b) Type B-5, and (c) Type C-2.

Table 2. Measured bridge heights and capacitance values of the switches.

Type	g	$C_{up,meas}$	$C_{d,meas}$	$C_{d,meas}/C_{d,sim}$	$C_{d,meas}/C_{up,meas}$
A-1	2.5 μm	38.5 fF	650 fF	0.37	16.8
A-2	2.1 μm	69.8 fF	926 fF	0.33	13.2
B-1	2.5 μm	38.5 fF	597 fF	0.34	15.5
B-2	2.5 μm	38.5 fF	597 fF	0.34	15.5
B-3	2.5 μm	38.5 fF	667 fF	0.38	17.3
B-4	2 μm	90 fF	1.05 pF	0.3	13
B-5	2 μm	90 fF	945 fF	0.27	10.5
C-1	5 μm	39 fF	1.12 pF	0.32	28.7
C-2	11 μm	30 fF	2.08 pF	0.37	69.3

parameters for the Type A-2, Type B-5, and Type C-2 switches, verifying that the proposed circuit model agrees well with the measurement results. The upstate capacitance and the bridge inductance values are in good agreement with the expressions in Section 3. The downstate capacitances are lower than the simulated values, the reasons of which will be explained below.

4.2. Evaluation of the Switch Performances

The results given in Table 2 show that the Type A and B switches have bridge heights about 2–2.5 μm and a down/up capacitance ratio of about 15. The measured downstate capacitance is about 30–40% of the simulated values. The decrease of downstate capacitance in the measurements is also raised by other researchers due to surface roughness of isolation dielectric [5]. The decrease of the downstate capacitance shifts the frequency bands of the switches from high to low; however, the circuit model and the expressions given in Section 3 are still valid for all of the switches. The first measurement results of the fabricated switches show that due to low spring constant [17], the Type C switches are more vulnerable to stiction due to dielectric charging and humidity. The structures are annealed in the oven at 200 °C for 15 minutes after the release process in order to enhance the restoring capability of the Type C switches. Although the annealing step solves the restoring problem of the Type C switches, it causes an increase in the bridge heights due to the sensitivity of meander structures to any annealing process step. The increase in the bridge height also increases the down/up capacitance ratio. The Type C-2 switch has the best down/up capacitance ratio, which is about 70. The switch has return loss better than 30 dB in the 1–20 GHz band. Its isolation is better than 20 dB between 11.1 GHz and 17.3 GHz, covering nearly the whole Ku-band, which is consistent with the formulation given in (2) and (3) for $C_{d,meas} = 2.08$ pF, and $L_b = 61.7$ pH. The switch has an insertion loss lower than 0.4 dB up to 20 GHz.

Some preliminary tests are done to evaluate the lifetime and failure modes of the fabricated RF MEMS switches. The outcomes of dielectric charging, both screening and stiction are also observed in this study similar to the ones in literature [18–21]. It is observed that the failure of the switches due to dielectric charging is determined not only by the number of cycles but also by the amplitude and waveform of the applied voltage. The switch structures in this work are tested in a lifetime setup up to 80×10^6 cycles with a bipolar actuation waveform [1].

5. CONCLUSION

This paper presents an empirical formulation for the bridge inductance of inductively tuned RF MEMS shunt switches, allowing a systematic design approach to tune their isolation bands. The isolation parameter is a very critical parameter in RF MEMS switches, and this parameter can be tuned with the use of recesses in the ground plane and meanders on the bridge, which may enhance the inductance by about 10 times compared to the conventional designs, allowing us to tune the isolation band to frequencies ranging from the X-band to the mm-wave band. The relationship between the bridge inductance and physical dimensions is extracted empirically to obtain analytical expressions for bridge inductance ranging up to 61.7 pH. The validity of the circuit model and the empirical formulation is verified with the measurements on the fabricated switches using the in-house RF MEMS process. The measurement results show that increasing the bridge inductance is a proper way of tuning the isolation characteristics of capacitive shunt switches. The formulation proposed in this work can be used in the design of inductively tuned RF MEMS capacitive shunt switches with the resonant frequencies ranging from X- to even Ka-band.

REFERENCES

1. Rebeiz, G. M., *RF MEMS Theory, Design, and Technology*, John Wiley & Sons, Hoboken, NJ, 2003.

2. Brown, E. R., "RF-MEMS switches for reconfigurable integrated circuits," *IEEE Trans. Microwave Theory and Tech.*, Vol. 46, No. 11, 1868–1880, Nov. 1998.

3. Afrang, S. and E. Abbaspour-Sani, "A low voltage MEMS structure for RF capacitive switches," *Progress In Electromagnetics Research*, PIER 65, 157–167, 2007.

4. Muldavin, J. B. and G. M Rebeiz, "High isolation CPW MEMS

shunt switches, Part I: Modeling," *IEEE Trans. Microwave Theory and Tech.*, Vol. 48, No. 6, 1045–1052, Jun. 2000.

5. Muldavin, J. B. and G. M Rebeiz, "High isolation CPW MEMS shunt switches, Part II: Design," *IEEE Trans. Microwave Theory and Tech.*, Vol. 48, No. 6, 1053–1056, Jun. 2000.

6. Tan, G. L. and G. M. Rebeiz, "DC-26 GHz MEMS series-shunt absorptive switches," *IEEE Int. Microwave Symp. Dig.*, 325–328, 2001.

7. Malczewski, A., S. Eshelman, B. Pillans, J. Ehmke, and C. L. Goldsmith, "X-band RF MEMS phase shifters for phased array applications," *IEEE Microwave Wireless Comp. Lett.*, Vol. 9, 517–519, Dec. 1999.

8. Kim, H.-T., S. Jung, K. Kang, J.-H. Park, Y.-K. Kim, and Y. Kwon, "Low-loss analog and digital micromachined impedance tuners at the Ka-band," *IEEE Trans. Microwave Theory and Tech.*, Vol. 49, No. 12, 2394–2400, Dec. 2001.

9. Monti, G., R. De Paolis, and L. Tarricone, "Design of a 3-state reconfigurable CRLH transmission line based on MEMS switches," *Progress In Electromagnetics Research*, PIER 95, 283–297, 2009.

10. Erdil, E., K. Topalli, M. Unlu, O. Aydin Civi, and T. Akin, "Frequency tunable microstrip patch antenna using RF MEMS technology," *IEEE Trans. Antennas and Propagation*, Vol. 55, 1193–1196, Apr. 2007.

11. Wu, W., B. Z. Wang, and S. Sun, "Pattern reconfigurable microstrip patch antenna," *Journal of Electromagnetic Waves and Applications*, Vol. 19, No. 1, 107–113, 2005.

12. Li, L. and D. Uttamchandani, "Demonstration of a tunable RF MEMS bandpass filter using silicon foundry process," *Journal of Electromagnetic Waves and Applications*, Vol. 23, No. 2–3, 405–413, 2009.

13. Peroulis, D., S. Pacheco, and L. P. B. Katehi, "MEMS devices for high isolation switching and tunable filtering," *IEEE Int. Microwave Symp. Dig.*, 1217–1220, 2000.

14. Topalli, K., O. Aydin Civi, S. Demir, S. Koc, and T. Akin, "A monolithic phased array using 3-bit DMTL RF MEMS phase shifters," *IEEE Trans. Microwave Theory and Tech.*, Vol. 56, No. 2, 270–277, Feb. 2008.

15. Simons, R. N., *Coplanar Waveguide Circuits, Components and Systems*, John Wiley & Sons, New York, 2001.

16. Goel, A. K., *High-Speed VLSI Interconnections: Modeling, Analysis, and Simulation*, Wiley, New York, 1994.

17. Pacheco, S. P., L. P. B. Katehi, and C. T.-C. Nguyen, "Design of low actuation voltage RF MEMS switch," *2000 IEEE MTT-S Int. Microwave Symp. Dig.*, 165–168, Boston, MA, Jun. 2000.

18. Goldsmith, C., J. Ehmke, A. Malczewski, B. Pillans, S. Eshelman, Z. Yao, J. Brank, and M. Eberly, "Lifetime characterization of capacitive RF MEMS switches," *IEEE Int. Microwave Symp. Dig.*, 227–230, 2001.

19. De Wolf, I., W. M. Van Spengen, R. Modlinski, A. Jourdain, A. Witvrouw, P. Fiorini, and H. A. C. Tilmans, "Reliability and failure analysis of RF MEMS switches," *Proc. 28th International Symposium for Testing and Failure Analysis (ISTFA2002)*, 275–281, 2002.

20. Melle, S., D. De Conto, D. Dubuc, K. Grenier, O. Vendier, J. L. Muraro, J.-L. Cazaux, and R. Plana, "Reliability modeling of capacitive RF MEMS," *IEEE Trans. Microwave Theory and Tech.*, Vol. 53, No.11, 3482–3488, Nov. 2005.

21. Van Spengen, W. M., R. Puers, R. Mertens, and I. De Wolf, "Experimental characterization of stiction due to charging in RF MEMS," *Int. IEEE Electron. Devices Meeting Dig.*, 901–904, 2002.